K^+p Phase-Shift Analysis below 1500 MeV/c*

A. T. LEA
Rutherford High Energy Laboratory, Chilton, Berkshire, England

AND

B. R. MARTIN
Brookhaven National Laboratory, Upton, New York

AND

G. C. OADES†
CERN, Geneva, Switzerland

(Received 25 August 1967)

An extensive systematic energy-dependent phase-shift analysis in the kaon laboratory momentum range 140–1495 MeV/c has been made of K^+p scattering data, supplemented by information from K^+p forward dispersion relations. S, P, and D waves were included, and various assumptions were made concerning the source of the inelasticity. Results are presented for solutions allowing all possible combinations of up to three partial waves to be inelastic. Four basic types of solution are found, and experiments are suggested which will best help to decide among them. Two of these groups of solutions show some evidence for a resonance in the $P_{1/2}$ partial wave, although its precise characteristics cannot be determined with present data.

1. INTRODUCTION

THE existence of a wealth of accurate experimental pion-nucleon scattering data has enabled several groups[1,2] to perform extensive phase-shift analyses up to a momentum of about 2 BeV/c. These analyses have confirmed much that was known about the πN system, and have, in addition, disclosed many interesting phenomena hitherto unsuspected. These discoveries have revitalized the phase-shift analysis technique, and have shown that, when used in conjunction with other techniques, it can be a powerful device to aid our knowledge of scattering phenomena.

With the successes in the πN field it is natural to attempt to apply similar methods to other systems and, in particular, to KN scattering. Unlike K^-p scattering, early experiments on K^+p scattering failed to discover the presence of any significant structure. However, in a recent series of accurate total cross-section measurements Cool *et al.*[3] have presented evidence for structure in the region of 1250-MeV/c kaon laboratory momentum. If this structure is associated with a resonance in the K^+p system it could not be incorporated into an $SU(3)$ multiplet of dimensionality less than 27. There are also difficulties in the quark model since at least 5 quarks would be needed to construct an object with the correct quantum numbers. Thus it is important to determine whether the structure observed in the total cross section is associated with a resonance in the K^+p system. Furthermore, since K^+p scattering is the only simple strange-particle system directly accessible to experiment which is not plagued by multichannel problems at low momenta, a knowledge of the K^+p phase shifts could help greatly in theoretical analyses of the KN interaction.

For these reasons we have made an extensive systematic phase-shift analysis of K^+p scattering data in the kaon laboratory momentum range 140–1495 MeV/c, the range being dictated by the availability of experimental data. In this paper we report on the results obtained from an energy-dependent analysis. In a subsequent paper we will report on further work on this system.

In Sec. 2 we outline the formalism, including the electromagnetic corrections, and in Sec. 3 we present a critical discussion of the data used in the analysis. In Sec. 4 we discuss phase-shift ambiguities and their possible resolution by the use of forward dispersion relations. Section 5 is devoted to a brief discussion of the possible inelastic channels available to the K^+p system, and in Sec. 6 is discussed the parametrization used and the search procedure followed. The results are presented and discussed in Secs. 7 and 8. Section 9 is devoted to conclusions and outlook. Finally, details of Legendre fits to the differential cross sections are given in Appendix A, and Appendix B contains details of the data sets used.

2. FORMULATION

A. Basic Equations for Measurable Quantities

The K^+p state is pure $I=1$, and so we will denote partial-wave amplitudes by $L_{I,2J}$, i.e., S_{11}, P_{11}, P_{13}, etc.,

* Work supported in part by the U. S. Atomic Energy Commission.

† Address from October 1967: Rutherford High Energy Laboratory, Chilton, Berkshire, England.

[1] L. D. Roper, R. M. Wright, and B. T. Feld, Phys. Rev. 138, B190 (1965).

[2] B. H. Bransden, R. G. Moorhouse, and P. O'Donnell, Phys. Rev. 139, B1566 (1965); Phys. Letters 19, 420 (1965); P. Auvil, C. Lovelace, A. Donnachie, and A. T. Lea, *ibid.* 12, 76 (1964); J. Cence, *ibid.* 20, 306 (1966); A. Donnachie, R. Kirsopp, A. T. Lea, and C. Lovelace, in *Proceedings of the Thirteenth Annual International Conference on High-Energy Physics* (University of California Press, Berkeley, Calif., 1967); A. Yokosawa, S. Suwa, R. E. Hill, R. J. Esterling, and N. E. Booth, Phys. Rev. Letters 16, 714 (1966).

[3] R. L. Cool *et al.*, Phys. Rev. Letters 17, 102 (1966).

where $J=l\pm\frac{1}{2}$ is the total angular momentum of the system. Natural units, such that $\hbar=m_\pi=c=1$, are used throughout this paper. The spin decomposition of the scattering amplitudes is exactly the same as for πN scattering[4] which, for completeness, we briefly outline below.

If we denote by $g(s,\theta)$ the spin-flip amplitude, and by $f(s,\theta)$ the non-spin-flip amplitude, then these are given by

$$f(s,\theta)=\sum_{l=0}^{\infty}[(l+1)f_{l+}(s)+lf_{l-}(s)]P_l(\cos\theta), \quad (1)$$

$$g(s,\theta)=i\sum_{l=1}^{\infty}[f_{l+}(s)-f_{l-}(s)]P_l^1(\cos\theta), \quad (2)$$

where s is the square of the total center-of-mass energy, θ is the center-of-mass scattering angle, $P_l(\cos\theta)$ and $P_l^1(\cos\theta)$ are the ordinary and associated Legendre polynomials, and $f_{l\pm}(s)$ is the partial-wave amplitude with total angular momentum $J=l\pm\frac{1}{2}$. The latter amplitudes may be expressed in terms of complex phase shifts $\alpha_{l\pm}(s)$ by

$$f_{l\pm}(s)=\frac{\exp[2i\alpha_{l\pm}(s)]-1}{2iq}=\frac{\eta_{l\pm}(s)\exp[2i\delta_{l\pm}(s)]-1}{2iq}, \quad (3)$$

where

$$\eta_{l\pm}(s)=\exp[-2\,\mathrm{Im}\alpha_{l\pm}(s)],$$
$$\delta_{l\pm}(s)=\mathrm{Re}\alpha_{l\pm}(s),$$

and q is the center-of-mass momentum.

The relevant measureable quantities may be expressed directly in terms of f and g, or $f_{l\pm}(s)$, as follows[5]:

(i) Differential cross section for unpolarized target:

$$(d\sigma/d\Omega)=|f(s,\theta)|^2+|g(s,\theta)|^2. \quad (4)$$

(ii) Recoil proton polarization for unpolarized target:

$$\mathbf{P}(s,\theta)=\frac{2\,\mathrm{Re}[f^*(s,\theta)g(s,\theta)]\hat{n}}{d\sigma(s,\theta)/d\Omega}, \quad (5)$$

where

$$\hat{n}=\frac{(\mathbf{q}\times\mathbf{q}')}{|(\mathbf{q}\times\mathbf{q}')|},$$

and q' is the center-of-mass momentum of the final kaon.

(iii) Forward real part:

$$\mathrm{Re}f(s,0)=\sum_{l=0}^{\infty}[(l+1)\,\mathrm{Re}f_{l+}(s)+l\,\mathrm{Re}f_{l-}(s)]. \quad (6)$$

(iv) Total cross section:

$$\sigma_T(s)=\frac{4\pi}{q}\sum_{l=0}^{\infty}[(l+1)\,\mathrm{Im}f_{l+}(s)+l\,\mathrm{Im}f_{l-}(s)]. \quad (7)$$

(v) Inelastic cross section,

$$\sigma_{\mathrm{in}}(s)=\sigma_T(s)-4\pi\sum_{l=0}^{\infty}[(l+1)|f_{l+}(s)|^2+l|f_{l-}(s)|^2]. \quad (8)$$

B. Electromagnetic Corrections

The scattering data which we have used are, in general, not corrected for electromagnetic effects. These corrections are important only for scattering in an angular range near to the forward direction, the range decreasing with increasing momentum. Practically all the effect of the electromagnetic interaction may be included by using those terms which may be expressed as additive corrections to the amplitudes $f(s,\theta)$ and $g(s,\theta)$ of Eqs. (1) and (2). A prescription which is nonrelativistically correct to all orders in α, the fine-structure constant, and relativistically correct to first order in α has been given by Roper *et al.*[1] We shall use that method here. Thus, relativistic electromagnetic (REM) amplitudes for K^+p scattering correct to first order in α are

$$f_{\mathrm{REM}}=\frac{-\alpha}{2W(1-\cos\theta)}\left\{\frac{W-m}{E-m}+\frac{W+m}{E+m}\cos\theta-(\mu_p-1)\times\left[\frac{W-E}{m}(1-\cos\theta)+\frac{E-m}{2m}\sin^2\theta\right]\right\}, \quad (9)$$

$$g_{\mathrm{REM}}=\frac{\alpha\sin\theta}{2W(1-\cos\theta)}\left\{\frac{W+m}{E+m}+(\mu_p-1)\left[\frac{2W-E+m}{2m}+\frac{E-m}{2m}\cos\theta\right]\right\}, \quad (10)$$

where E is the center-of-mass energy of the proton, W is the total center-of-mass energy ($W=\sqrt{s}$), and μ_p is the proton's total magnetic moment in nuclear magnetons. Nonrelativistic (Coulomb) amplitudes correct to all orders in α are

$$f_{\mathrm{Coul}}=\frac{-\alpha[E(W-E)+q^2]}{q^2W(1-\cos\theta)}\times\exp\left\{\frac{-i\alpha[E(W-E)+q^2]}{qW}\ln\left(\frac{1-\cos\theta}{2}\right)\right\}, \quad (11)$$

$$g_{\mathrm{Coul}}=0. \quad (12)$$

These Coulomb amplitudes contain the nonrelativistic electromagnetic amplitudes to first order in α, which are

[4] See e.g., J. Hamilton and W. S. Woolcock, Rev. Mod. Phys. **35**, 737 (1963).

[5] See e.g., O. T. Vik and H. R. Rugge, Phys. Rev. **129**, 2311 (1963); and Ref. 2.

also contained in Eqs. (9) and (10). The common terms are

$$f_{\mathrm{Coul}\,\alpha}=\frac{-\alpha[E(W-E)+q^2]}{q^2W(1-\cos\theta)}, \tag{13}$$

$$g_{\mathrm{Coul}\,\alpha}=0. \tag{14}$$

Thus the total electromagnetic corrections which are independent of the nuclear phases are

$$f_{\mathrm{EM}}=f_{\mathrm{REM}}+f_{\mathrm{Coul}}-f_{\mathrm{Coul}\,\alpha}, \tag{15}$$

$$g_{\mathrm{EM}}=g_{\mathrm{REM}}, \tag{16}$$

and these are to be added to the nuclear amplitudes [given by Eqs. (1) and (2)] to give the total amplitudes, f and g.

The above corrections are adequate for our purposes because (i) most of the differential cross sections are not measured very close to the forward direction. In the three cases where there is an angular point with $\cos\theta>0.95$, the errors on the data are such as to render a more accurate correction unnecessary. (ii) The corrections we ignore are always estimated to be less than 1°, and our final phases are rarely predicted to that accuracy. Furthermore, inclusion of the general form of the corrections would either greatly increase the computer storage necessary, or, alternatively, increase the time of computation considerably.

3. EXPERIMENTAL DATA

The main bulk of the experimental data consists of total cross sections and elastic differential cross sections, with, in addition, a few inelastic cross sections, and a few values for the recoil proton polarization. The data are distributed fairly uniformly in the region 140–1500 MeV/c but there is a large gap from 1500–2000 MeV/c in which no angular distributions have been measured. Consequently we have restricted our analysis to the region below 1500 MeV/c. We discuss below the data in the region 140–1495 MeV/c and the corrections which we have included in our analysis.

A. Total Cross Section

Prior to the publication of the data of Cool *et al.*,[3] the K^+p total cross section was only poorly known. The data available up to 850 MeV/c consisted of some very early emulsion results[6] and three points[7] (at 457, 522, and 589 MeV/c) from a counter experiment. Both of these sets of data disagree with more recent total cross sections calculated from the differential cross sections of Goldhaber *et al.*,[8] and have not been included in our analysis. Between 850 and 1495 MeV/c very accurate data are now available.[3] Other data in this region,[9–12] although less accurate, are consistent with the data of Cool *et al.*[3] and are included in the analysis.

To summarize the situation, accurate data are now available from 850–2000 MeV/c, but below this region there are still no accurate measurements. An independent set of measurements below 850 MeV/c would be very useful in order to provide a basis for the absolute normalization of differential cross-section data in this region.

B. Inelastic Cross Section

Between the threshold for single pion production (525 MeV/c) and 2 BeV/c there are only nine measurements of the total inelastic cross section.[8,9,13–16] Since the available data indicate quite rapid changes in the inelastic cross section over this momentum range, more data is clearly required. Furthermore, an accurate knowledge of the inelastic cross section provides an important constraint on possible sets of phase shifts.

C. Differential Cross Section

Prior to the phase-shift analysis we analyzed the differential cross-section data in terms of Legendre-polynomial expansions. This gave information which enabled us to remove obvious inconsistencies in the data, and also determine the highest number of partial waves required to fit the data. In Appendix A we give details of these fits together with a graph of the Legendre series coefficients. We give here a discussion of all the differential cross-section data available together with comments on the corrections we found necessary.

1. Below 300 MeV/c

Because of the large forward peak caused by Coulomb scattering, no attempt was made to fit this data with Legendre polynomials. The differential cross sections at 140, 175, 205, 235, and 265 MeV/c (Ref. 8) were included unaltered in our analysis to provide a low-energy constraint on the phase shifts.

2. 355, 520, and 642 MeV/c

These remaining three low-energy differential cross sections of the Goldhaber group[8] are well fitted by a two-

[6] D. Keefe *et al.*, Nuovo Cimento **12**, 241 (1959).
[7] T. F. Kycia, L. T. Kerth, and R. G. Baender, Phys. Rev. **118**, 553 (1960).
[8] S. Goldhaber *et al.*, Phys. Rev. Letters **9**, 135 (1962).
[9] T. F. Stubbs *et al.*, Phys. Rev. Letters **7**, 188 (1961).
[10] V. Cook *et al.*, Phys. Rev. Letters **7**, 182 (1961); Phys. Rev. **129**, 2743 (1963).
[11] H. C. Burrowes *et al.*, Phys. Rev. Letters **2**, 117 (1959).
[12] A. Bettini *et al.*, Phys. Letters **16**, 83 (1965).
[13] W. Chinowsky, G. Goldhaber, S. Goldhaber, T. O'Halloran, and B. Schwarzschild, Phys. Rev. **139**, B1411 (1965).
[14] T. A. Filippas *et al.* (to be published).
[15] E. Barrelet (to be published).
[16] R. W. Bland *et al.*, Phys. Rev. Letters **17**, 939 (1966); in *Proceedings of the Thirteenth Annual International Conference on High-Energy Physics* (University of California Press, Berkeley, Calif., 1967).

parameter Legendre-polynomial expansion. This is consistent with our assumption of the dominance of s waves at low momenta.

3. 522 MeV/c

This counter experiment[7] gave fairly large errors on the differential cross-section values. In order to bring it into general agreement with the more recent data at 520 MeV/c[8] the points were renormalized to 90% of their quoted values. It was also found necessary after the first fits to rebin the points at $\cos\theta=-0.423$ and -0.574 into one point at $\cos\theta=-0.499$.

4. 778 MeV/c

This recent bubble-chamber experiment[17] has very good statistics. However, our Legendre series fits indicated that it was necessary to rebin the four points at $\cos\theta=-0.35$, -0.45, -0.55, and -0.65 into two points at $\cos\theta=-0.4$ and -0.6.

5. 810 MeV/c

The results of this early bubble-chamber experiment[9] are reasonably well fitted by a three-term Legendre series.

6. 910 MeV/c

This propane bubble-chamber experiment[18] was mainly intended to measure the recoil proton polarization. Some differential cross-section data were also produced and they are well fitted by a three-term Legendre series.

7. 970 and 1170 MeV/c

Both of these sets of spark-chamber data[10] are reasonably well fitted by three-term Legendre polynomial expansions. In the 970-MeV/c set it was found necessary to rebin the points at $\cos\theta=0.4$ and 0.6 into one point at $\cos\theta=0.5$.

8. 1450 MeV/c

This comprehensive counter experiment[12] is well fitted by a five-term Legendre series.

In addition to the data listed above, there are preliminary data from four bubble-chamber experiments.

9. 735 MeV/c

The Legendre fits indicated that it was advisable to rebin the data completely from intervals of 0.1 in $\cos\theta$ to intervals of 0.2.

[17] S. Focardi *et al.*, Phys. Letters **24**, B314 (1967).
[18] W. Hirsch and G. Gidal, Phys. Rev. **135**, B191 (1964).

10. 860, 960, and 1200 MeV/c

This preliminary data[19] is well fitted by three- or four-term Legendre series expansions. We have renormalized the data slightly in order to bring it into line with the most recent total cross-section measurements of Cool *et al.*[20]

D. Recoil Proton Polarization

To date there have only been two measurements of the recoil proton polarization. There are four points at 910 MeV/c[18] and three preliminary points at 778 MeV/c.[21] The values at 910 MeV/c have been changed in sign to agree with the conventional definition of positive polarization.[22]

To summarize the data situation, in the momentum range up to 1 BeV/c, there are 16 sets of elastic differential cross-section data of which only 4 have average errors of less than 10%. Between 1 BeV/c and 1.5 BeV/c there are 3 sets, of which 2 have good statistics. There are now very accurate total cross-section measurements above 850 MeV/c, but below this momentum the total cross-section data is poor. The situation for inelastic cross sections and recoil proton polarization measurements is very bad, there being a mere 8 points of the former and 7 of the latter.

From the above it is clear that the K^+p data situation is far from good. In order, in the future, that the K^+p situation be comparible to that of πN scattering, it would be necessary to have complete sets of data, i.e., differential cross sections, recoil proton polarizations, and independent measurements of the total and inelastic cross sections, at momentum intervals of about 50 MeV/c. We appreciate the experimental difficulties that this would involve, particularly at low momenta.

4. PHASE-SHIFT AMBIGUITIES AND FORWARD DISPERSION RELATIONS

In Sec. 3 we have seen that the available experimental data consist mainly of total and differential cross sections. Fitting only such data can lead, *at a given momenta*, to several ambiguities.[23] A second solution may be obtained from the true solution by interchanging partial waves of the same J value but with opposite parities. This is the Minami ambiguity.[24] Then there is the sign ambiguity[25] where a third solution may be

[19] R. W. Bland *et al.*, quoted by G. Goldhaber in University of California Radiation Laboratory Report No. UCRL-17388 (unpublished); see also Ref. 16.
[20] T. F. Kycia (private communication).
[21] F. Femino, S. Iannelli, F. Messanares, L. Monari, and P. Serra, Nuovo Cimento (to be published).
[22] We are grateful to Dr. V. P. Henri for pointing out this change in sign.
[23] See e.g., L. D. Roper and D. S. Bailey, Phys. Rev. **155**, 1744 (1967).
[24] S. Minami, Progr. Theoret. Phys. (Kyoto) **11**, 213 (1954).
[25] See e.g., H. A. Bethe and F. de Hoffmann, *Mesons and Fields* (Row Peterson & Co., New York, 1955), Vol. 2, p. 70.

obtained by simultaneously reversing the signs of the real parts of all the phase shifts. In addition, a combination of these two transformations can produce a fourth solution.[23]

The measurements of Goldhaber *et al.*[8] at low momenta showed that Coulomb interference fixed the sign of the real part of the forward scattering amplitude as negative, thus removing the sign ambiguity. They then showed that the differential cross sections could be fitted with a dominant repulsive S_{11} phase. Applying the Minami transformation we see that there is a second solution with a dominant repulsive P_{11} phase. Besides these two solutions there is a third solution, the Yang[26] ambiguity of the second. This is a mixture of an attractive P_{11} phase and a larger repulsive P_{13} phase. Goldhaber *et al.*[8] favored the dominant repulsive S_{11} phase shift on the grounds that the energy dependence of the phase was proportional to q rather than q^3, thus excluding a simple p-wave type threshold behavior. This situation has also been discussed by Ino,[27] who finds that a theoretical study of the forces in this system favors the S_{11} dominant solution. In our analysis we have assumed that the dominant repulsive S_{11} solution is correct at low momenta. At higher momenta, however, the phase shifts may have changed sufficiently rapidly for both ambiguities to be present.

From Eqs. (1)–(8) it can be seen that although the total and elastic differential cross sections remain invariant under the sign and Minami transformations, the forward real part will change sign under both transformations. Thus to resolve these ambiguities requires both recoil proton polarization data and values for the real parts of the forward scattering amplitude.

In our analysis we have included values for the real part of the forward scattering amplitude as calculated from a K^+p forward-dispersion relation subtracted once at threshold. The inclusion of the forward real parts thus resolves the sign ambiguity, but since there are so few values of the recoil proton polarization the possibility still remains of Minami-type ambiguities at higher momenta.

If we denote by $f_\pm(\nu)$ the forward amplitude for $K^\pm p$ scattering at a total kaon laboratory energy ν, a dispersion relation subtracted once at threshold is

$$\mathrm{Re}f_+(\nu)=\mathrm{Re}f_+(m_K)$$
$$-\sum_Y \frac{(\nu-m_Y)R_Y}{(\nu+\nu_Y)(\nu_Y+m_K)}-\frac{(\nu-m_K)}{4\pi^2}\mathcal{P}\int_{m_K}^{\infty}d\nu' k'$$
$$\times\left[\frac{\sigma_-(\nu')}{(\nu'+\nu)(\nu'+m_K)}-\frac{\sigma_+(\nu')}{(\nu'-\nu)(\nu'-m_K)}\right]$$
$$-\frac{(\nu-m_K)}{\pi}\int_{\nu_{\pi Y}}^{m_K}d\nu'\frac{\mathrm{Im}f_-(\nu')}{(\nu'+\nu)(\nu'+m_K)}, \quad (17)$$

where

$$\nu_Y=\frac{m_Y^2-m^2-m_K^2}{2m}$$

and

$$R_Y=\frac{(m_Y-m)^2-m_K^2}{4mm_Y}\frac{g_Y^2}{4\pi}.$$

The kaon laboratory momentum is k', and m_Y and g_Y are the masses and coupling constants of the hyperons Y (Λ^0 and Σ^0) to the $\bar{K}N$ channel.

The physical integral in (17) was evaluated using known total cross sections below 19 BeV/c,[28] and a Regge-pole model above this momentum. The Regge-pole parameters deduced by Rarita and Phillips[29] were used for the latter part of the calculation. The subtraction constant was evaluated by using the s-wave scattering length of Goldhaber *et al.*[8] The integral in Eq. (17) involving the K^-p unphysical region was evaluated using a constant-scattering-length approximation to the Dalitz-Tuan[30] extrapolation procedure for the s waves, and a Lagrangian method for the p-wave $Y_1^*(1385)$ contribution with an $SU(3)$ coupling.[31] This treatment of the K^-p unphysical region is rather crude. However, although a far better treatment of this region is necessary if one is to deduce accurate values for g_Y,[32] its contribution to the forward real part in the region below 1.5 BeV/c is rather small for the particular dispersion relation we have used.

At a given momentum, a range of values of $\mathrm{Re}f_+(\nu)$ was found by taking into account the error on the s-wave K^+p scattering length,[8] by using different sets of K^-p scattering lengths in the unphysical region,[33] and by varying the values of the KYN coupling constants between their $SU(3)$ values [taking the $SU(3)$ mixing parameter $\alpha=\frac{2}{3}$], and the small values obtained by Lusignoli *et al.*[34] The extremities of the range of values obtained were used to define the "error" on the forward real part for the purpose of the analysis. The major part of this error comes from the error on the s-wave K^+p scattering length.

5. INELASTIC CHANNELS

The main features of the total and partial inelastic cross sections for K^+p scattering in this region are shown

[26] See e.g., G. Källen, *Elementary Particle Physics* (Addison-Wesley Publishing Co., Inc., Mass., 1964).
[27] T. Ino, Progr. Theoret. Phys. (Kyoto) **37**, 398 (1967).
[28] W. Galbraith *et al.*, Phys. Rev. **138**, B913 (1965); W. F. Baker *et al.*, *ibid.* **129**, 2285 (1963); A. N. Diddens, E. W. Jenkins, T. F. Kycia, and K. F. Riley, *ibid.* **132**, 2721 (1963); M. B. Watson, M. Ferro-Luzzi, and R. D. Tripp, *ibid.* **131**, 2248 (1963); O. Chamberlain *et al.*, *ibid.* **125**, 1696 (1962); P. Nordin, *ibid.* **123**, 2168 (1961); see also Refs. 3 and 8–13.
[29] R. J. N. Phillips and W. Rarita, Phys. Rev. **139**, B1336 (1965).
[30] R. H. Dalitz and S. F. Tuan, Ann. Phys. (N. Y.) **10**, 307 (1960).
[31] R. L. Warnock and G. Frye, Phys. Rev. **138**, B947 (1965).
[32] See e.g., H. P. C. Rood, Nuovo Cimento **50**, A493 (1967).
[33] J. K. Kim, Phys. Rev. Letters **14**, 29 (1965); M. Sakitt *et al.*, Phys. Rev. **139**, B719 (1965).
[34] M. Lusignoli, M. Restignoli, G. A. Snow, and G. Violini, Phys. Letters **21**, 229 (1966).

TABLE I. Possible main inelastic channels.

Inelastic channel $K^+p \rightarrow$	Production threshold[a] Kaon laboratory momentum (MeV/c)	Total c.m. energy (MeV)	Width of resonance in final state (MeV)	Contribution to initial state K^+p partial wave for final state in a relative s wave[b]	p wave[c]
$KN\pi$	525	1573		P_{11}	S_{11}, D_{13}
$\kappa(720)N$	715	1659	<12	P_{11}	S_{11}, D_{13}
$KN\pi\pi$	825	1711		S_{11}	P_{11}, P_{13}
$KN^*(1236)$	870	1732	120	D_{13}	P_{11}, P_{13}, F_{15}
$K^*(890)N$	1075	1829	50	S_{11}, D_{13}	P_{11}, P_{13}, F_{15}
$KN\sigma(410)$	1110	1845	?	S_{11}	P_{11}, P_{13}
$KN\pi\pi\pi$	1120	1849		P_{11}	S_{11}, D_{13}
$KN^*(1400)$	1220	1896	~200	S_{11}	P_{11}, P_{13}
$KN\eta(549)$	1417	1984	<0.01	P_{11}	S_{11}, D_{13}
$KN\pi\pi\pi\pi$	1422	1987		S_{11}	P_{11}, P_{13}
$Z_0(1865)\pi$	1460	2003	150	?	?
$K^*(1080)N$	1495	2019	?	?	?
$KN^*(1525)$	1500	2021	105	P_{13}	S_{11}, D_{13}, D_{15}

[a] Calculated at resonance mass.
[b] Relative s wave between all final particles.
[c] Relative p wave between two particles in final state, the rest being relative s waves.

qualitatively in Fig. 1. The total inelastic cross section rises sharply around 1 BeV/c and then increases more slowly to a value of about 11 mb at 2 BeV/c.

In Table I are shown details of possible inelastic processes. The threshold for single pion production is at 525 MeV/c, but the first measured value for the inelastic cross section is 0.06±0.03 mb at 642 MeV/c,[8] which shows that there is no rapid initial rise in this channel. At 870 MeV/c the production of $N^*(1236)$ can occur, and beyond this momentum the inelastic cross section rises quickly. Above 1075 MeV/c, $K^*(890)$ production also becomes possible and the two resonant states, $KN^*(1236)$ and $K^*(890)N$, then dominate the inelastic channels up to 1500 MeV/c.[16,19]

Table I also shows the initial K^+p states from which the various inelastic states can be produced in relative s or p waves. It can be seen that $N^*(1236)$ may be produced in a relative s state from the initial D_{13} K^+p state, and in a relative p state from initial P_{11}, P_{13}, and F_{15} states. $K^*(890)$ can be produced from the same states, and, in addition, production in a relative s state is also possible from an initial S_{11} K^+p state.

TABLE II. Fits to K^+p data with one wave inelastic.

Inelastic partial waves	N_{DF}	χ^2	χ^2/N_{DF}
	(a) Published K^+p data		
S_{11}	202	2791.5	13.82
P_{11}	202	1689.1	8.36
P_{13}	199	621.9	3.13
D_{13}	201	685.9	3.41
D_{15}	197	354.9	1.80
	(b) All K^+p data		
S_{11}	333	4149.3	12.46
P_{11}	333	2952.7	8.87
P_{13}	330	962.3	2.92
D_{13}	332	1091.3	3.29
D_{15}	328	648.4	1.98

A preliminary analysis of $KN^*(1236)$ production data by Bland *et al.*[16,19] indicates that there is roughly equal production from P_{11} and P_{13} K^+p initial states with an additional contribution, increasing rapidly with momentum, from a state of opposite parity.

6. PARAMETRIZATIONS AND SEARCH PROCEDURE

An initial survey of the available data and the single-energy phase-shift analyses that had been made to date led us to the conclusion that, at this stage, a multi-energy analysis would be the most useful approach.

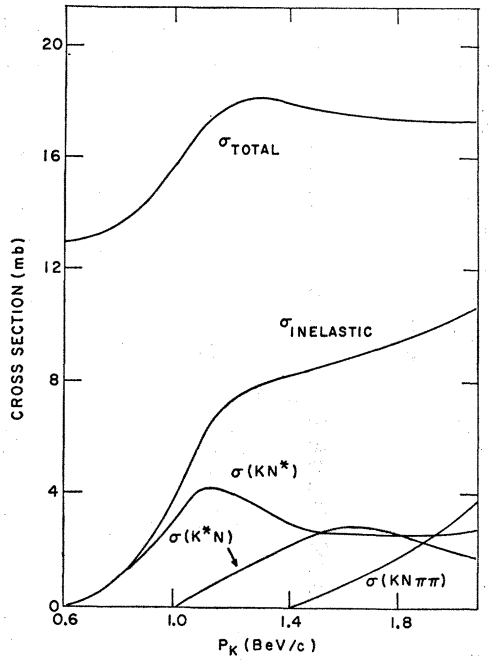

FIG. 1. Qualitative behavior of the total and partial K^+p cross sections.

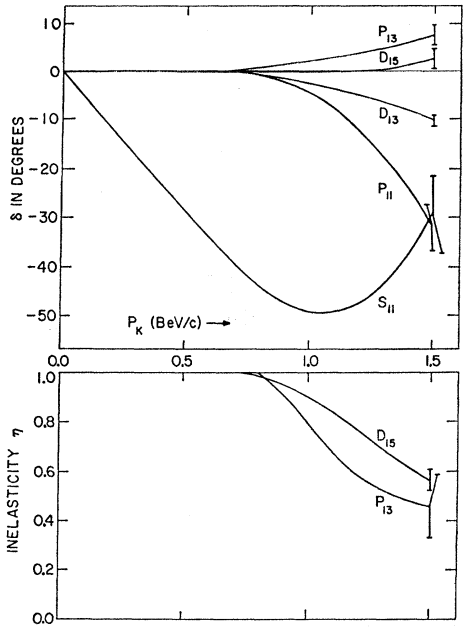

FIG. 2. Phases and inelasticities for solution $P_{13}D_{15}$ (ii) of Table III(a).

After some preliminary trials the following parametrizations were used for the real part of the phase shift δ, and the inelasticity factor η:

$$\delta_l = q^{2l+1}(A_l + B_l q^2 + C_l q^4), \qquad \eta_l = (1+y_l^2)^{-1}, \tag{18}$$

TABLE III. Fits to K^+p scattering data with two waves inelastic.

Inelastic partial waves	N_{DF}	χ^2	χ^2/N_{DF}	Probability %
(a) Published K^+p data				
$S_{11}P_{11}$	199	769.6	3.89	0.00
$S_{11}P_{13}$	199	283.1	1.43	0.01
$S_{11}D_{13}$	198	318.4	1.61	0.00
$S_{11}D_{15}$	198	278.6	1.41	0.01
$P_{11}P_{13}$ (i)	199	414.5	2.09	0.00
(ii)	199	417.1	2.11	0.00
$P_{11}D_{13}$	198	221.1	1.12	12.48
$P_{11}D_{15}$	198	253.2	1.28	0.49
$P_{13}D_{13}$	198	236.3	1.19	3.25
$P_{13}D_{15}$ (i)	198	187.9	0.95	68.50
(ii)	198	176.0	0.89	86.72
$D_{13}D_{15}$ (i)	197	337.4	1.70	0.00
(ii)	197	319.8	1.62	0.00
(b) All K^+p data				
$S_{11}P_{11}$	330	1257.3	3.82	0.0
$S_{11}P_{13}$	330	540.3	1.64	0.0
$S_{11}D_{13}$	329	556.7	1.69	0.0
$S_{11}D_{15}$	329	554.0	1.68	0.0
$P_{11}P_{13}$ (i)	330	774.9	2.36	0.0
(ii)	330	740.9	2.25	0.0
$P_{11}D_{13}$	329	453.1	1.38	0.0
$P_{11}D_{15}$	329	453.5	1.38	0.0
$P_{13}D_{13}$	329	451.7	1.37	0.0
$P_{13}D_{15}$ (i)	329	419.6	1.28	0.05
(ii)	329	384.3	1.17	1.91
$D_{13}D_{15}$ (i)	328	651.1	1.98	0.00
(ii)	328	617.8	1.88	0.00

TABLE IV. Fits to K^+p scattering data with three waves inelastic.

Inelastic partial waves	N_{DF}	χ^2	χ^2/N_{DF}	Probability %
(a) Published K^+p data				
$S_{11}P_{11}P_{13}$	199	211.2	1.06	23.37
$S_{11}P_{11}D_{13}$	199	182.0	0.92	80.13
$S_{11}P_{11}D_{15}$	199	294.0	1.48	0.00
$S_{11}P_{13}D_{13}$	199	187.8	0.94	70.47
$S_{11}P_{13}D_{15}$	199	180.4	0.91	82.30
$S_{11}D_{13}D_{15}$	199	333.4	1.68	0.00
$P_{11}P_{13}D_{13}$ (i)	199	247.4	1.24	1.11
(ii)	198	180.5	0.91	80.84
$P_{11}P_{13}D_{15}$	199	233.5	1.17	4.73
$P_{11}D_{13}D_{15}$ (i)	199	190.3	0.96	65.78
(ii)	197	184.0	0.93	73.81
(iii)	197	176.3	0.90	85.25
$P_{13}D_{13}D_{15}$	199	185.1	0.93	75.18
(b) All K^+p data				
$S_{11}P_{11}P_{13}$	330	403.0	1.22	0.37
$S_{11}P_{11}D_{13}$	330	378.9	1.15	3.28
$S_{11}P_{11}D_{15}$	330	530.7	1.61	0.00
$S_{11}P_{13}D_{13}$	330	419.6	1.27	0.06
$S_{11}P_{13}D_{15}$	330	396.2	1.20	0.72
$S_{11}D_{13}D_{15}$	330	613.3	1.86	0.00
$P_{11}P_{13}D_{13}$ (i)	330	481.5	1.46	0.00
(ii)	329	395.4	1.20	0.70
$P_{11}P_{13}D_{15}$	330	464.7	1.41	0.00
$P_{11}D_{13}D_{15}$ (i)	330	388.1	1.18	1.52
(ii)	328	370.9	1.13	5.14
(iii)	328	369.5	1.13	5.69
$P_{13}D_{13}D_{15}$	330	402.0	1.22	0.41

where

$$y_l = \theta(s-s_T)\left(\frac{s-s_T}{s}\right)^{3/2}\left[D_l + E_l\left(\frac{s-s_T}{s}\right)\right],$$

and $\theta(s-s_T)$ is usual (0,1) step function. The available

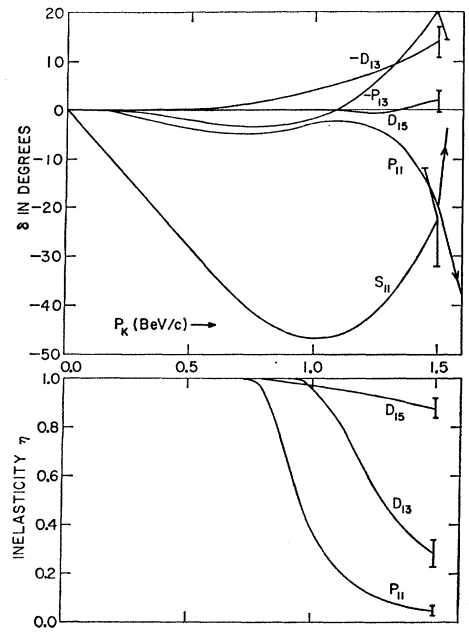

FIG. 3. Phases and inelasticities for solution $P_{11}D_{13}D_{15}$ (iii) of Table IV(a).

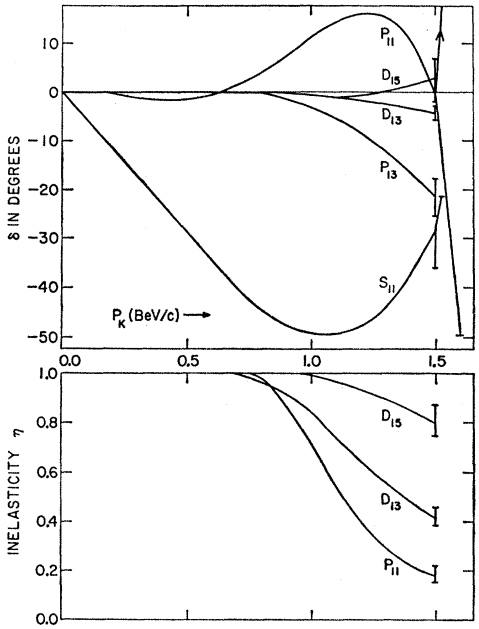

FIG. 4. Phases and inelasticities for solution $P_{11}D_{13}D_{15}$ (iii) of Table IV(b).

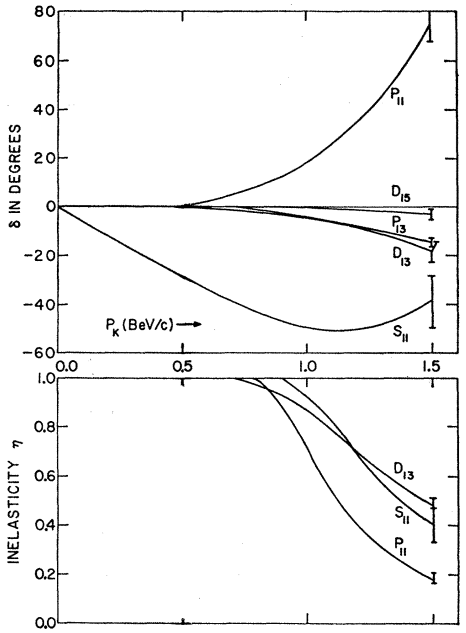

FIG. 6. Phases and inelasticities for solution $S_{11}P_{11}D_{13}$ of Table IV(b).

data are not sufficiently accurate to determine the precise form of η_l at low momenta just above the inelastic threshold. The form used was found to be adequate.

For a given partial wave there is thus a maximum of six parameters, A_l, B_l, and C_l for the real part of the phase shift, and D_l, E_l, and s_T for the inelasticity factor. The parametrization was chosen mainly for its simplicity and not for any particular physical reason, the only physical restriction on the parameters being the requirement that s_T be greater than the first inelastic threshold.

The parameters were varied to minimize

$$\chi^2=\sum_{\text{all data}}\left(\frac{D_{\text{expt}}-D_{\text{param}}}{\Delta D_{\text{expt}}}\right)^2, \tag{19}$$

where ΔD_{expt} is the experimental error on the data point D_{expt}, and D_{param} is the corresponding value obtained from the parametrization. We will quote results either in terms of χ^2/N_{DF} (where $N_{\text{DF}}=N_D-N_P$ is the number of degrees of freedom, N_D being the total number of data and N_P the number of parameters) or $P(\chi^2,N_{\text{DF}})$, the corresponding probability.

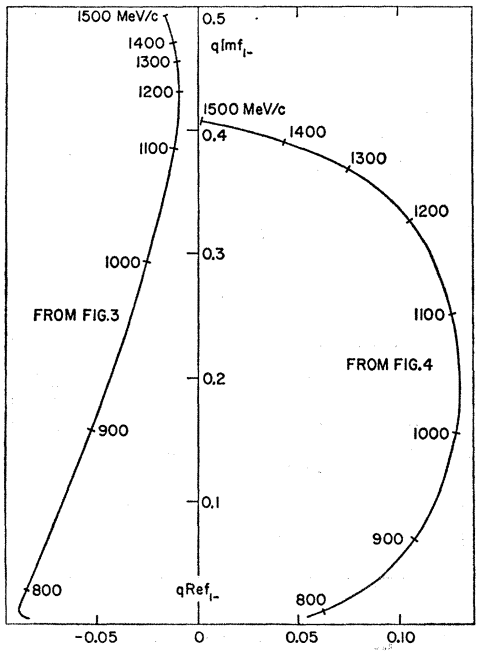

FIG. 5. Adair plot for solutions shown in Figs. 3 and 4.

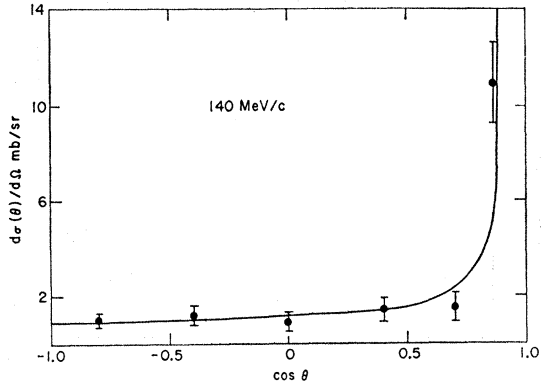

FIG. 7. Fit to the elastic differential cross section at 140 MeV/c from solution $P_{11}D_{13}D_{15}$ (iii) of Table IV(b).

TABLE V. Phases at 1495 MeV/c as determined by all the K^+p data (δ in degrees).

Type	χ^2/N_{DF}	S_{11} δ	S_{11} η	P_{11} δ	P_{11} η	P_{13} δ	P_{13} η	D_{13} δ	D_{13} η	D_{15} δ	D_{15} η
Group I											
$P_{11}D_{13}D_{15}$ (iii)	1.13	−29.3	1.00	0.5	0.19	−22.0	1.00	−4.9	0.43	2.6	0.81
$P_{11}D_{13}D_{15}$ (ii)	1.13	−23.8	1.00	7.1	0.19	−21.7	1.00	13.0	0.75	−11.2	0.63
$S_{11}P_{13}$	1.64	−64.7	0.29	−19.1	1.00	13.4	0.12	−19.5	1.00	−3.3	1.00
D_{15}	1.98	−13.5	1.00	−1.6	1.00	−35.4	1.00	2.4	1.00	−15.6	0.33
Group II											
$S_{11}P_{11}D_{13}$	1.15	−38.8	0.40	72.4	0.19	−15.3	1.00	−17.6	0.48	−3.4	1.00
$P_{11}D_{13}D_{15}$ (i)	1.18	−23.4	1.00	59.6	0.15	−17.1	1.00	10.0	0.60	−13.3	0.75
$P_{11}P_{13}D_{13}$ (ii)	1.20	−30.5	1.00	59.8	0.13	−19.5	0.72	−4.9	0.46	−2.5	1.00
$S_{11}P_{11}P_{13}$	1.22	−50.4	0.21	123.4	0.12	−19.3	0.58	−17.4	1.00	−4.5	1.00
$P_{11}D_{13}$	1.38	−20.7	1.00	94.3	0.05	−24.0	1.00	−6.0	0.19	−0.2	1.00
Group III											
$P_{11}D_{15}$	1.38	−26.8	1.00	9.9	0.33	−28.3	1.00	10.1	1.00	−7.3	0.53
$P_{11}P_{13}D_{15}$	1.41	−37.8	1.00	18.8	0.16	−19.7	0.63	1.0	1.00	−8.5	0.72
$S_{11}P_{11}D_{15}$	1.61	−28.9	0.89	11.6	0.18	−24.2	1.00	8.2	1.00	−10.1	0.53
$S_{11}D_{15}$	1.68	−22.9	0.66	12.5	1.00	−33.1	1.00	3.1	1.00	−15.2	0.49
$D_{13}D_{15}$ (ii)	1.88	−22.2	1.00	5.0	1.00	−34.0	1.00	12.1	0.55	−8.3	0.68
Group IV											
$P_{13}D_{15}$ (ii)	1.17	−35.0	1.00	−30.4	1.00	10.3	0.37	−7.6	1.00	0.3	0.66
$S_{11}P_{13}D_{15}$	1.20	−41.0	0.73	−22.5	1.00	11.7	0.25	−5.0	1.00	−6.6	0.74
$P_{13}D_{13}D_{15}$	1.22	−33.7	1.00	−25.8	1.00	10.7	0.27	−7.8	0.94	−2.3	0.70
$S_{11}P_{13}D_{13}$	1.27	−52.3	0.45	−21.6	1.00	9.5	0.24	−13.2	0.76	−4.4	1.00
$P_{13}D_{15}$ (i)	1.28	−43.4	1.00	−7.2	1.00	−22.8	0.47	−6.3	1.00	6.7	0.62
$P_{13}D_{13}$	1.37	−30.4	1.00	−38.3	1.00	3.3	0.39	−15.1	0.55	2.1	1.00
$P_{11}P_{13}D_{13}$ (i)	1.46	−36.3	1.00	−29.4	0.79	0.4	0.32	−11.9	0.59	0.1	1.00
$S_{11}D_{13}$	1.69	−17.5	0.56	−52.7	1.00	−6.4	1.00	−16.2	0.21	−6.2	1.00
$S_{11}D_{13}D_{15}$	1.86	−16.5	0.57	−49.5	1.00	−3.6	1.00	−18.4	0.22	−3.7	0.90
$D_{13}D_{15}$ (i)	1.98	−23.9	1.00	−49.0	1.00	−10.0	1.00	−9.8	0.59	4.0	0.62

The Legendre-polynomial fits (see Appendix A) show that above 1 BeV/c, d waves are expected to be present. Thus we have included the five partial waves S_{11}, P_{11}, P_{13}, D_{13}, and D_{15}. Since one of the objects of the present work is to determine the minimum number of parameters needed to fit the data, we have performed analyses under the assumptions that (i) only one wave is inelastic (5 combinations), (ii) only two waves are inelastic (10 combinations), and (iii) only three waves are inelastic (10 combinations). For each of the above choices about 100 minimizations were made from general trial solutions, their only common feature being a negative s-wave phase shift at very low momenta. The resulting solutions were then sorted into different types, and several of the best of each type subjected to further

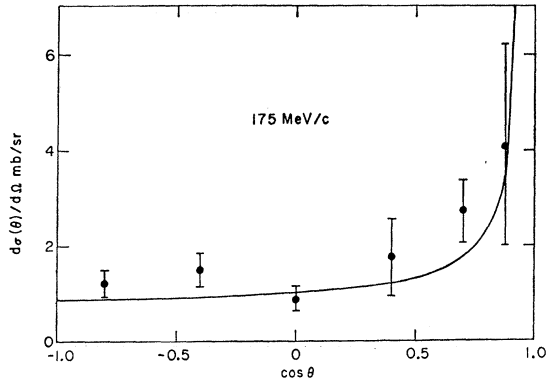

FIG. 8. Fit to the elastic differential cross section at 175 MeV/c from solution $P_{11}D_{13}D_{15}$ (iii) of Table IV(b).

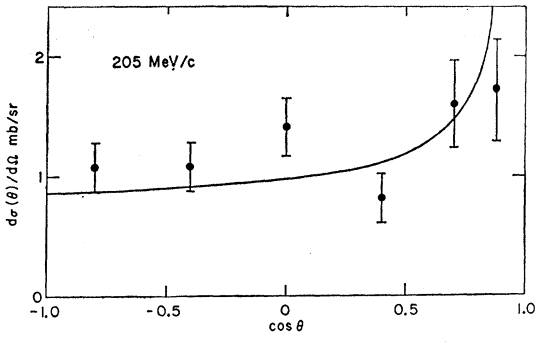

FIG. 9. Fit to the elastic differential cross section at 205 MeV/c from solution $P_{11}D_{13}D_{15}$ (iii) of Table IV(b).

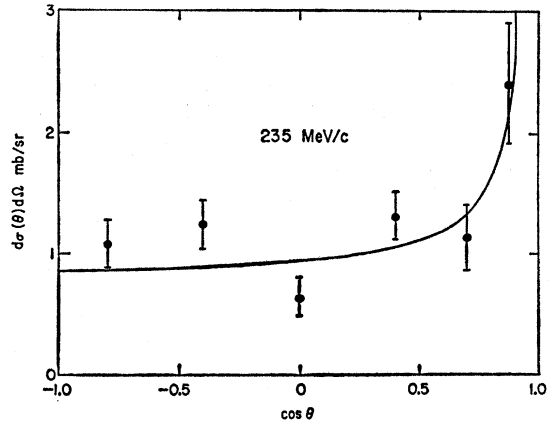

FIG. 10. Fit to the elastic differential cross section at 235 MeV/c from solution $P_{11}D_{13}D_{15}$ (iii) of Table IV(b).

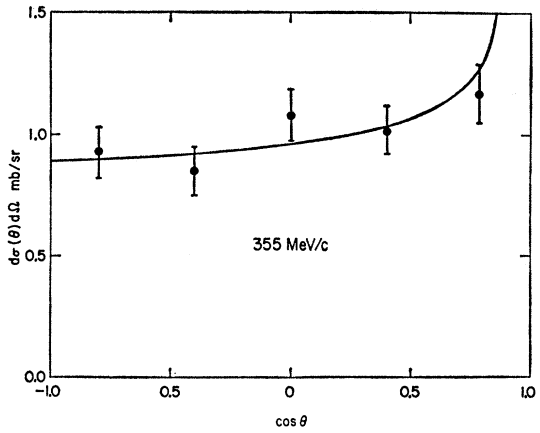

FIG. 12. Fit to the elastic differential cross section at 355 MeV/c from solution $P_{11}D_{13}D_{15}$ (iii) of Table IV(b).

extensive searching. The best solutions of each of the latter groups were used for final minimizations.

7. RESULTS

We have made our analyses using two data sets, details of which are given in Appendix B. The first set consists of published data in the range 140–1495 MeV/c and has a total of 214 data points. The second set contains, in addition, the preliminary differential cross-section data at 735,[15] 860, 960, and 1200 MeV/c,[16,17] and preliminary recoil proton polarization data at 778 MeV/c.[21] This latter set has a total of 345 data points. Details of the best solutions obtained under our various assumptions concerning inelasticity are given below.

A. One Wave Inelastic

Table II shows the minimum values of χ^2 obtained for the five possible cases using the two data sets. The most interesting feature is that, with the exception of the very slight increase in the case of D_{13}, χ^2 falls as the inelasticity is ascribed to a higher partial wave. The main reason for the bad fits is that it is impossible to simultaneously fit the higher-momenta differential cross sections and also reproduce the rapid rise in the inelastic cross section. The improvement in χ^2 as the inelasticity moves to a higher partial wave is due to the fact that higher partial waves contribute more to the inelastic cross section.

B. Two Waves Inelastic

Table III shows the minimum values of χ^2 obtained for the ten possible combinations of two inelastic partial waves. The main features to emerge from these searches are that all solutions in which S_{11} is inelastic are bad, the case of $S_{11}P_{11}$ being the worst of all. Closer examination of this particular combination shows that, as in the case of one wave inelastic, it is unable to fit the rapid rise in the inelastic cross section.

For the combinations $P_{11}P_{13}$, $P_{13}D_{15}$, and $D_{13}D_{15}$ two solutions appeared in each case, both solutions having comparible values for χ^2. The best fit to the published data having two waves inelastic was given by solution $P_{13}D_{15}$ (ii), and we will see in the Sec. 8 that this solution is marginally better than even the best solution with

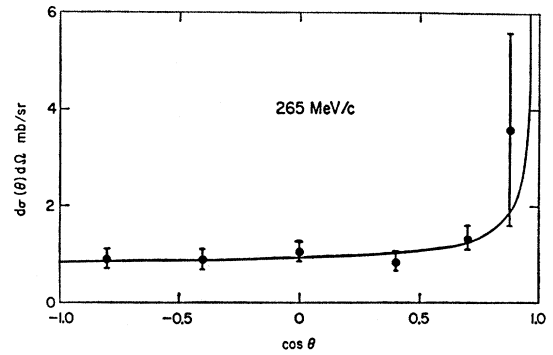

FIG. 11. Fit to the elastic differential cross section at 265 MeV/c from solution $P_{11}D_{13}D_{15}$ (iii) of Table IV(b).

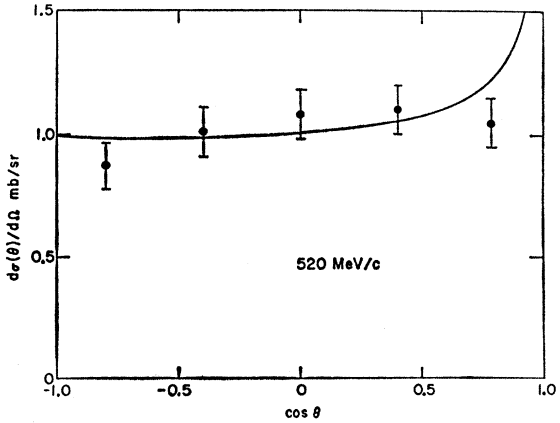

FIG. 13. Fit to the elastic differential cross section at 520 MeV/c from solution $P_{11}D_{13}D_{15}$ (iii) of Table IV(b).

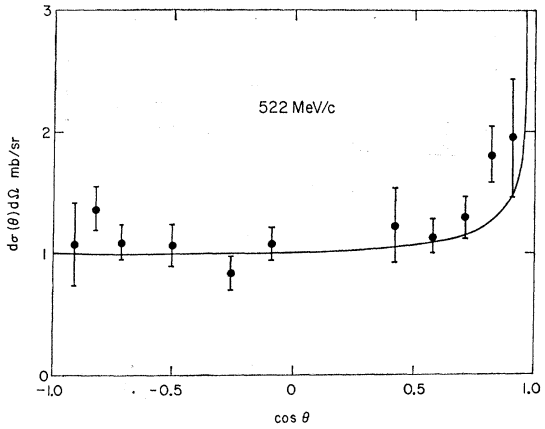

FIG. 14. Fit to the elastic differential cross section at 522 MeV/c from solution $P_{11}D_{13}D_{15}$ (iii) of Table IV(b).

three waves inelastic. When the preliminary data was also included this solution still survived as the best solution with two inelastic waves, but now some solutions with three waves inelastic gave better fits to this complete data set.

Figure 2 shows the characteristics of this solution as determined by the published data. The corresponding solution determined by all the data is very similar. One interesting feature is that both P_{13} and D_{15} show signs

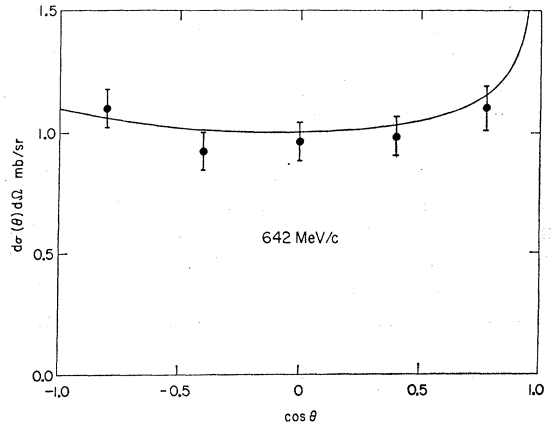

FIG. 15. Fit to the elastic differential cross section at 642 MeV/c from solution $P_{11}D_{13}D_{15}$ (iii) of Table IV(b).

of the Ball-Frazer[35] mechanism, the real part of the phase shift increasing as the partial wave becomes more inelastic.

C. Three Waves Inelastic

Table IV shows the minimum values of χ^2 obtained for the ten possible combinations of three inelastic partial waves. The first point of interest is that, when only the published data is used, 6 of the 10 possible combinations give solutions with probabilities greater than 50%. In the case of the combination $P_{11}P_{13}D_{13}$ two solutions appeared, while for $P_{11}D_{13}D_{15}$ three solutions were found. The best fit to the published data is given by solution $P_{11}D_{13}D_{15}$ (iii), although, as noted above, $P_{13}D_{15}$ (ii) gives an even better fit. When the preliminary data is also included this solution with three inelastic waves still gives the best fit and, moreover, is now the best of all the solutions having either one, two, or three waves inelastic.

Figure 3 shows this best solution $P_{11}D_{13}D_{15}$ (iii), as determined by the published data while Fig. 4 shows this same solution when the preliminary data is also

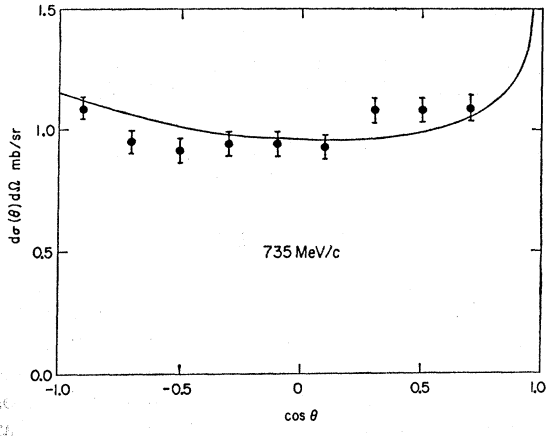

FIG. 16. Fit to the elastic differential cross section at 735 MeV/c from solution $P_{11}D_{13}D_{15}$ (iii) of Table IV(b).

included in the fit. The main change is in the behavior of the real part of the P_{11} phase. In both cases it starts negative but begins to turn as the inelasticity starts to increase. In the first case this turn-around is only slight and is not enough to bring the real part of the phase shift positive, but in the second case it is much stronger, δ passing through 0° at about 650 MeV/c and reaching a maximum value of 15.5° at about 1200 MeV/c. After this rise both solutions show a fall in δ.

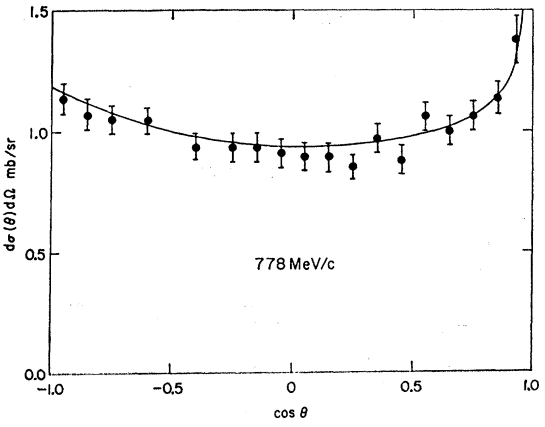

FIG. 17. Fit to the elastic differential cross section at 778 MeV/c from solution $P_{11}D_{13}D_{15}$ (iii) of Table IV(b).

[35] J. S. Ball and W. R. Frazer, Phys. Rev. Letters 7, 204 (1961).

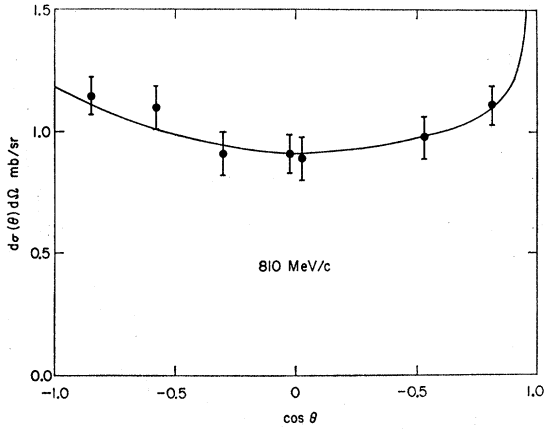

FIG. 18. Fit to the elastic differential cross section at 810 MeV/c from solution $P_{11}D_{13}D_{15}$ (iii) of Table IV(b).

These two solutions are interesting since they illustrate the difficulties in distinguishing between a simple Ball-Frazer mechanism and a true inelastic resonance. In the solution shown in Fig. 3 the real part of the P_{11} phase is initially negative. However, once inelasticity sets in η drops very quickly with a corresponding rise in δ. Then, as the inelasticity levels off, the real part of the phase turns again and falls. In the solution shown in

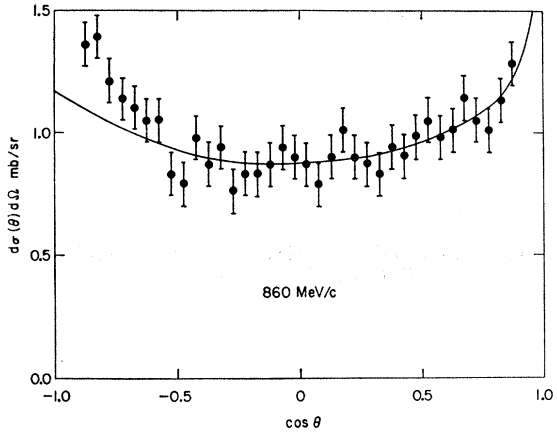

FIG. 19. Fit to the elastic differential cross section at 860 MeV/c from solution $P_{11}D_{13}D_{15}$ (iii) of Table IV(b).

Fig. 4 the inelasticity falls nearly as quickly, but now the positive bump in δ is much more marked. Figure 5 shows the Adair[36] plot for these two cases. The second curve shows very clearly the behavior of an inelastic resonance, possibly superimposed on an attractive background, whereas such an interpretation in the case of the first curve is much less obvious.

8. DISCUSSION OF RESULTS

We shall now discuss in more detail the results obtained when we fit the second data set in which the preliminary data is included as well as the published data. Although this data set is not as well fitted as when the preliminary data is removed, nevertheless we feel that these solutions are more reliable, the decrease in probability being due to the inherent difficulties of energy-dependent phase-shift analyses rather than to inconsistencies in the data.

In Table V we show values for the phases and inelasticities at 1495 MeV/c for all solutions having χ^2/N_{DF} less than 2.0. This excludes seven solutions which, since they also have $\chi^2/N_{\mathrm{DF}}>2.0$ when only the published data is used, we believe are unrealistic.

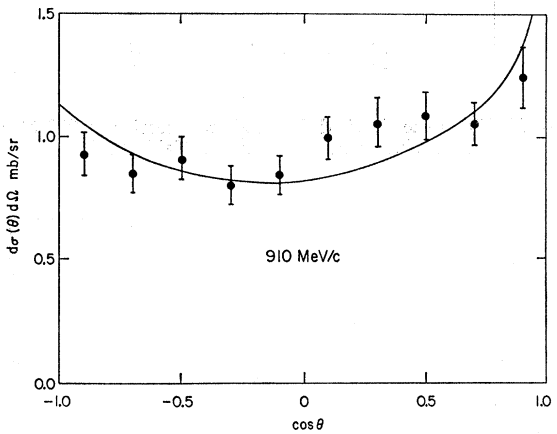

FIG. 20. Fit to the elastic differential cross section at 910 MeV/c from solution $P_{11}D_{13}D_{15}$ (iii) of Table IV(b).

The behavior of δ for S_{11} is roughly similar in every case and is consistent with our assumption of a Goldhaber type (S_{11} repulsive and dominant) low-energy solution. If we classify the solutions according to the behavior of δ for P_{11} we see that the solutions may be divided into four groups. In group I, δ rises and then falls through 0°. In the case of the first two solutions of this group this behavior is accompanied by a rapid fall in η for P_{11}; the typical behavior of an inelastic resonance. In the case

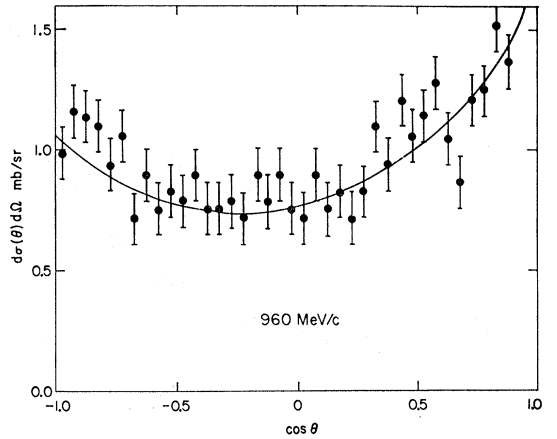

FIG. 21. Fit to the elastic differential cross section at 960 MeV/c from solution $P_{11}D_{13}D_{15}$ (iii) of Table IV(b).

[36] R. K. Adair, Phys. Rev. 113, 338 (1959).

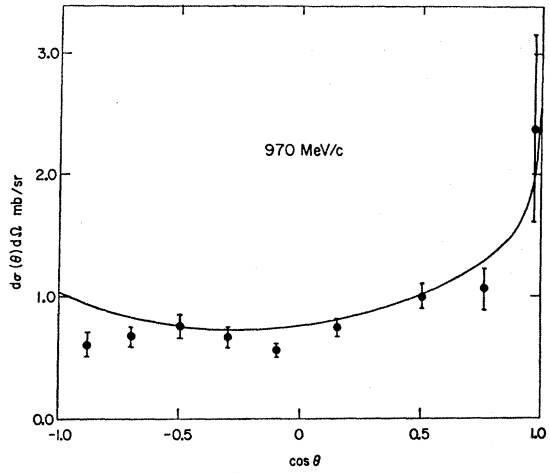

FIG. 22. Fit to the elastic differential cross section at 970 MeV/c from solution $P_{11}D_{13}D_{15}$ (iii) of Table IV(b).

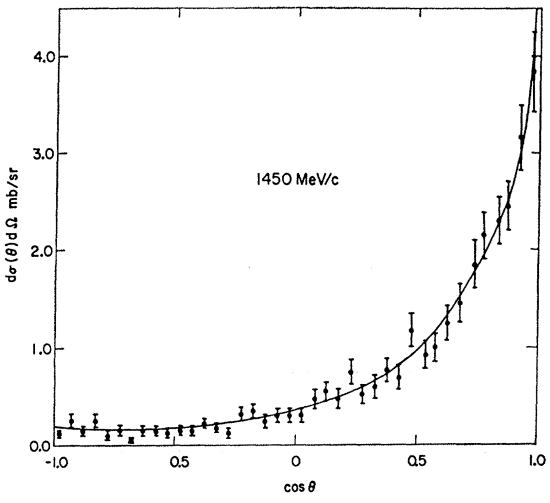

FIG. 25. Fit to the elastic differential cross section at 1450 MeV/c from solution $P_{11}D_{13}D_{15}$ (iii) of Table IV(b).

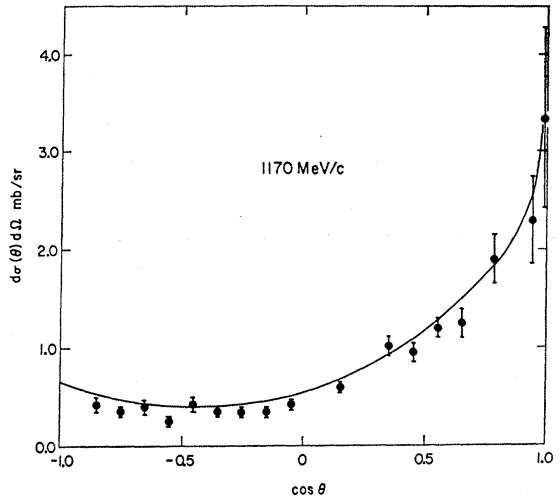

FIG. 23. Fit to the elastic differential cross section at 1170 MeV/c from solution $P_{11}D_{13}D_{15}$ (iii) of Table IV(b).

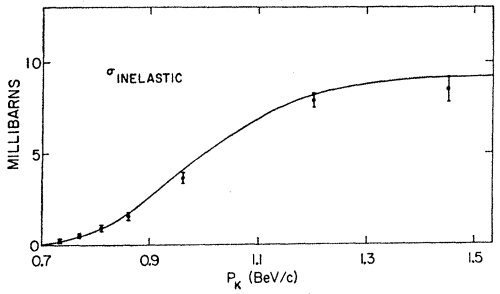

FIG. 26. Fit to the inelastic cross section from solution $P_{11}D_{13}D_{15}$ (iii) of Table IV(b).

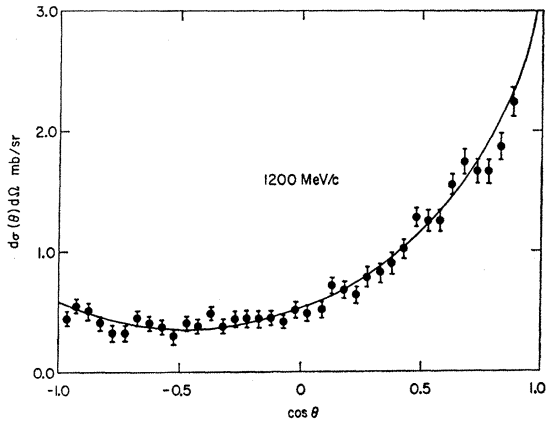

FIG. 24. Fit to the elastic differential cross section at 1200 MeV/c from solution $P_{11}D_{13}D_{15}$ (iii) of Table IV(b).

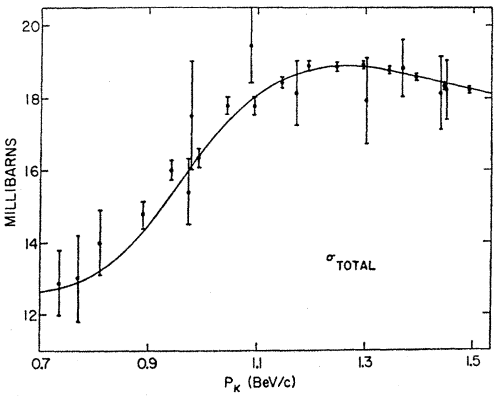

FIG. 27. Fit to the total cross section from solution $P_{11}D_{13}D_{15}$ (iii) of Table IV(b).

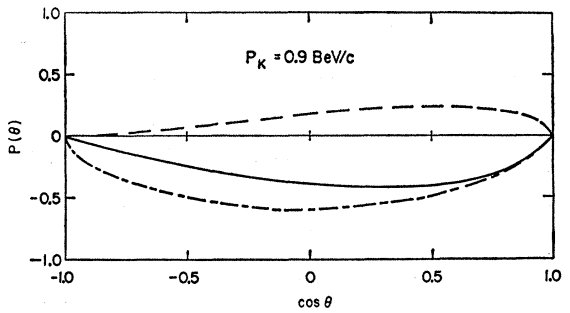

FIG. 28. Recoil proton polarization at 900 MeV/c as predicted by the best solution of groups I (solid line), II (dot-dashed line), and IV (dashed line).

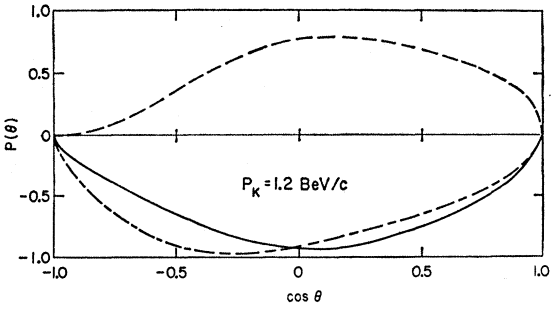

FIG. 29. Recoil proton polarization at 1200 MeV/c as predicted by the best solution of groups I (solid line), II (dot-dashed line), and IV (dashed line).

of the other two solutions P_{11} is elastic so we believe them to be unrealistic, this explaining the much larger values of χ^2. In group II, δ for P_{11} rises quickly and in two cases passes upward through 90°, a typical "normal" resonance behavior. Again for all members of this group the bulk of the inelasticity is in P_{11}. In group III, δ for P_{11} rises only slowly even though in the best three solutions η has fallen quickly. These solutions we find somewhat suspect since we would expect such a drop in η to produce signs of a Ball-Frazer mechanism in δ. Finally, in group IV, δ for P_{11} falls fairly slowly, P_{11} being elastic in all except one solution.

The behavior of the other phases are roughly consistent within each group. For groups I, II, and III, the bulk of the inelasticity is in P_{11} except for a few suspect solutions with large χ^2. In all except one case, δ for P_{13} falls slowly and this partial wave is elastic or else only slightly inelastic. The d waves are not very well determined. For group IV the bulk of the inelasticity is in P_{13} except for the three worst solutions. Also, apart from these three and one other solution, δ for P_{13} rises slowly, showing no signs of an inelastic resonance type behavior. Again the d waves are not well determined.

The statistically best solution is of group I and has been shown in Fig. 4. Thes best solution of group II we show in Fig. 6, while the best solution of group IV is very similar to that shown in Fig. 2, which gives the same solution as determined by the published data. We do not show a group-III solution since they are statistically far inferior to the best solutions of the other three groups.

The solutions of groups I and II are basically variants of one another in that they all show some form of resonance behavior in the P_{11} state. Since such a resonance appears to be in the region of 1500 MeV/c, better determination of whether it is elastic or inelastic and the values for its energy and width must await further accurate data in the region 1–2 BeV/c. It is nevertheless interesting that evidence for an enhancement in this region has been reported in both K^+p total cross section[37] and photoproduction experiments.[38] Solutions of group IV show no resonance behavior. A choice between these and solutions of groups I and II can be made on the basis of further accurate measurements in the region we have analyzed as we shall discuss below.

9. CONCLUSIONS AND OUTLOOK

We have presented the results of an extensive systematic energy-dependent phase-shift analysis of K^+p scattering below 1.5-BeV/c kaon laboratory momentum. The characteristics of the solutions found have enabled them to be classified into four main groups, the best solution of group III being statistically far inferior to those of the other groups. An interesting feature of the solutions of groups I and II is the possible existence of a resonance in the $P_{1/2}$ state.

In view of the multiplicity of solutions the question of most interest now is what additional experimental data could best help decide between them. Fits to all the cross-section data for the best solution of group I are shown in Figs. 7–27. The best solutions of groups II and IV produce fits which are very similar. In fact, at the low momenta they are indistinguishable. Thus only very accurate cross-section data in the range below 1.5 BeV/c could hope to distinguish between these solutions. However, this is not to say that additional data in this region are not potentially useful, since they could help to improve the accuracy of the existing solutions. In particular, more measurements of the total inelastic

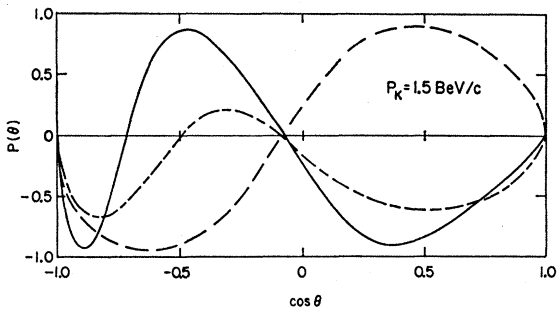

FIG. 30. Recoil proton polarization at 1500 MeV/c as predicted by the best solution of groups I (solid line), II (dot-dashed line), and IV (dashed line).

[37] R. J. Abrams *et al.*, Phys. Rev. Letters **19**, 259 (1967).
[38] J. Tyson *et al.*, Phys. Rev. Letters **19**, 255 (1967).

cross section would be very valuable. The differential cross sections predicted by the three types of solution when extrapolated above 1.5 BeV/c do differ, the differences increasing with momentum. However, to extrapolate phase shifts beyond a range where they are known to fit data is a dangerous procedure and we shall not pursue the point here.

There remains the question of the recoil proton polarization. In Figs. 28–30 are shown the predicted recoil proton polarizations from the best solutions of groups I, II, and IV. The differences are striking between the group-IV solution and the other two. It is also encouraging that the predicted polarizations are large. Thus measurements of the recoil proton polarization in the momentum range 1.0–1.5 BeV/c should clearly distinguish between resonant and nonresonant type solutions. However, if the former type are preferred, then somewhat more accuracy would be required to deduce the detailed characteristics of the resonance. We urge that such experiments be done.

Finally, as we mentioned in Sec. 3, there are no measurements of any angular distributions in the momentum range 1.5–2.0 BeV/c. In view of the possible existence of a $P_{1/2}$ resonance in this region, suggested by solutions of groups I and II, and the enhancements observed by two experimental groups,[37,38] it is important that angular distributions (both for elastic scattering and recoil proton polarizations) be measured in this momentum range.

ACKNOWLEDGMENTS

This work was started while two of us (ATL and BRM) were at the Niels Bohr Institute, Copenhagen, and the third author (GCO) was at NORDITA, Copenhagen. The first two authors wish to thank Professor A. Bohr for the hospitality of the Institute, and the Science Research Council (England) for the award of NATO fellowships. The third author similarly wishes to thank Professor C. Møller for the hospitality of NORDITA, and Turner and Newall for a research fellowship.

In addition, we wish to thank the following people for discussions and/or communicating data in numerical form or prior to publication: G. Goldhaber (Berkeley), J. Hamilton (NORDITA), V. P. Henri (CERN), P. B. Jones (Oxford), T. F. Kycia (Brookhaven), and R. F. Peierls (Brookhaven).

APPENDIX A: LEGENDRE-POLYNOMIAL FITS TO THE K^+p DIFFERENTIAL CROSS SECTIONS

The differential cross-section data were fitted with Legendre series[39] for two reasons: (i) to determine the maximum number of partial waves required at each momentum, and (ii) to remove obvious inconsistencies in the data.

We have used the series

$$\frac{d\sigma}{d\Omega}(s,\theta)=\sum_{n=0}^{N} c_n(s)P_n(\cos\theta), \qquad \text{(A1)}$$

and in order to present a systematic approach the following technique was used:

(i) The data were first fitted with a one-term series, then a two-term series, and so on up to a twelve-term series (or until the number of degrees of freedom fell to zero).

(ii) The fits were then inspected to see if any points were consistently giving large contributions to χ^2. Such points were subsequently rebinned, or rejected, and stage (i) repeat.

At this point two criteria can be applied to decide on where to truncate Eq. (A1). First, one can look for the

TABLE VI. Legendre fits to data at 735 MeV/c.

Number of terms	Original data N_{DF}	χ^2	χ^2/N_{DF}	$P(\chi^2)$ %	Data after alterations N_{DF}	χ^2	χ^2/N_{DF}	$P(\chi^2)$ %
1	18	62.3	3.46	0.00	8	18.2	2.28	1.95
2	17	55.3	3.25	0.00	7	15.4	2.19	3.17
3	16	38.7	2.42	0.12	6	4.8	0.79	57.00
4	15	24.9	1.66	5.20	5	2.1	0.41	83.53
5	14	24.4	1.74	4.07	4	2.1	0.52	71.74
6	13	23.6	1.81	3.55	3	1.4	0.47	70.55
7	12	22.8	1.90	2.91	2	1.3	0.64	52.20
8	11	19.0	1.64	6.11	1	0.2	0.22	66.00
9	10	18.0	1.80	5.46				
10	9	17.4	1.93	4.32				
11	8	13.5	1.69	9.61				
12	7	9.0	1.29	25.03				

TABLE VII. Details of the number of Legendre coefficients needed to fit the elastic differential cross sections.

Laboratory momentum (MeV/c)	Number of terms for a probability of 30%	Number of terms for 1st minimum in χ^2/N_{DF}
355	2	2
520	1	no minimum[a]
522	3	6
642	3	1
735	3	4
780	3	4
810	3	1
860	3	1
910	2	3
960	3	3
970	3	5
1170	3	3
1200	4	4
1450	5	6

[39] We are grateful to R. G. Kirsopp for making his Legendre series fitting program available to us.

[a] The first minimum is almost certainly lost because of a bad scatter of points.

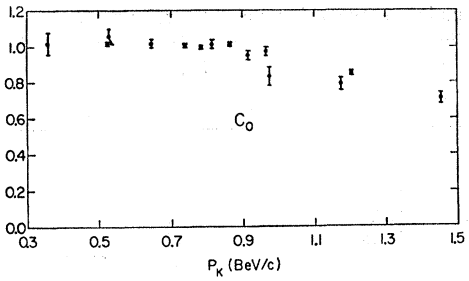

FIG. 31. Energy dependence of the Legendre coefficient C_0.

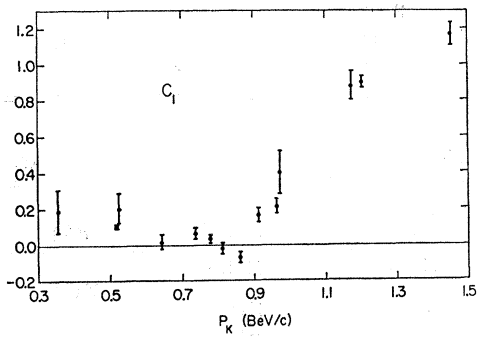

FIG. 32. Energy dependence of the Legendre coefficient C_1.

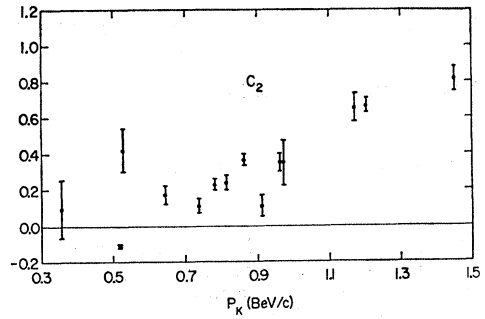

FIG. 33. Energy dependence of the Legendre coefficient C_2.

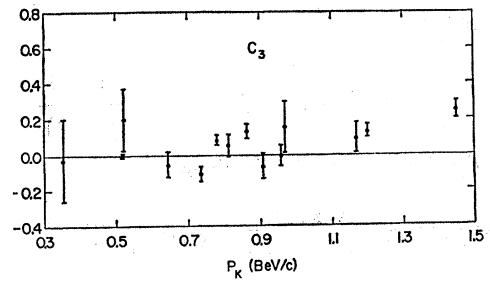

FIG. 34. Energy dependence of the Legendre coefficient C_3.

point where the probability exceeds 50% ($\chi^2/N_{DF}\simeq 1$), and, second, where the first minimum in χ^2/N_{DF} occurs. The first criterion means that on the average the data points are fitted to within the quoted errors, while the second criterion means that adding another term in the Legendre series does not significantly decrease χ^2. Ideally both criteria should be satisfied at the same point, but in practice they are usually not.

Let the probability exceed 50% for N_p terms in the series, and let the minimum in χ^2/N_{DF} occur for N_m terms. If the average number of terms needed to fit other experiments in the same energy region is N, then we would judge an individual fit to be good if

$$N=N_p\pm 1=N_m\pm 1.$$

We often find that while $N_m=N$, N_p is either very large or very small. If N_p is large, then there are either some isolated bad points or the over-all errors are too small and should be increased. If N_p is small, then conversely the errors are probably too large. In cases where $N_m\gg N$, it usually means that the first minimum in χ^2/N_{DF} has been lost due to rather bad data.

As an example of the use of the Legendre fitting technique, Table VI shows the 735-MeV/c [15] preliminary data both before and after rebinning. The original data gave a minimum in χ^2/N_{DF} for 4 terms but the corresponding probability was only 5.2%. Note that even with a 12-term series the probability only rises to 25%. After rejecting the point at $\cos\theta=0.85$ and rebinning the remaining data from intervals of 0.1 in $\cos\theta$ to intervals of 0.2, the first minimum in χ^2/N_{DF} still occurs for 4 terms while the probability rises above 50% for a series with three or more terms.

In Table VII we give details of the number of terms needed to satisfy both criteria after making the necessary adjustments to the data. Here we have used a probability of 30% as a criterion for a good fit because of the scatter on the data from some, particularly older, experiments. It will be seen that the highest number of terms are required for the 1450-MeV/c data. Here a term in $\cos^4\theta$ is required, indicating the presence of a d-wave term at this momentum.

In Figs. 31–34 we show the first four Legendre series coefficients as functions of laboratory momentum in the region from 335 to 1450 MeV/c. Values below 355 MeV/c are not shown because the Coulomb effects are large enough to influence the coefficients.

APPENDIX B: DETAILS OF THE DATA

In Tables VIII and IX we show details of both the published and preliminary data, respectively. The crosses indicate that the data have been included in the analysis, and the number in parentheses gives the reference.

The data are shown in Figs. 7–27 together with fits from the over-all best solution.

TABLE VIII. Published data included in first data set. The numbers in parentheses give the references.

Laboratory momentum (MeV/c)	σ_{tot}	σ_{inel}	Forward real part	$d\sigma/d\Omega$	$P(\theta)$	Laboratory momentum (MeV/c)	σ_{tot}	σ_{inel}	Forward real part	$d\sigma/d\Omega$	$P(\theta)$
140			X	X(8)		992	X(3)		X		
175			X	X(8)		1043	X(3)		X		
205			X	X(8)		1087	X(11)		X		
235			X	X(8)		1094	X(3)				
265			X	X(8)		1144	X(3)		X		
355			X	X(8)		1170	X(10)		X	X(10)	
520			X	X(8)		1194	X(3)		X		
522				X(7)		1245	X(3)		X		
642			X	X(8)		1295	X(3)				
770	X(10)		X			1300	X(10)		X		
778		X(14)		X(17)		1345	X(3)		X		
810	X(9)	X(9)	X	X(9)		1367	X(11)		X		
891	X(3)		X			1395	X(3)		X		
910			X	X(18)	X(18)	1440	X(10)				
942	X(3)		X			1445	X(3)				
970	X(10)		X	X(10)		1450	X(12)	X(12)	X	X(12)	
976	X(11)					1495	X(3)		X		

TABLE IX. Additional preliminary data included in second data set. The numbers in parentheses give the references.

Laboratory momentum (MeV/c)	σ_{tot}	σ_{inel}	Forward real part	$d\sigma/d\Omega$	$P(\theta)$
735	X(15)	X(15)	X	X(15)	
778					X(21)
860		X(19)	X	X(19)	
960		X(19)		X(19)	
1200		X(16)		X(19)	

PHYSICAL REVIEW VOLUME 165, NUMBER 5 25 JANUARY 1968

Test for $N^*(1400)$ Dominance of Nucleonic Form Factors

D. H. LYTH
Department of Physics, University of Lancaster, St. Leonard's Gate, Lancaster, England
(Received 26 June 1967)

By assuming that "nucleonic" form factors are dominated by the contribution of the $N^*(1400)$ resonance (which is the only object having the same quantum numbers as the nucleon), the relation $g_{\gamma NN}/g_{\pi NN} = g_{\gamma NN^*}/g_{\pi NN^*}$ is derived (the g's are coupling constants, and only magnetic coupling to the photon is considered). A recent phase-shift analysis of photoproduction off protons by Chau, Dombey, and Moorhouse gives a value for $g_{\gamma NN^*}$ agreeing in sign but twice too large.

IT has recently been implied[1] that nucleonic form factors might be dominated by the $N^*(1400)$ resonance (which has the same quantum numbers as the nucleon), just as electromagnetic form factors are dominated by vector mesons.[2] In this paper it is intended to confront this idea with experiment and to make some general comments on it.

The γNN and πNN vertices will be considered. With the photon and one nucleon on the mass shell, and the other nucleon off the mass shell (mass W), the γNN vertex is given by[3]

$$\langle p|J_\mu(0)|p'\rangle=\frac{\bar{u}(p)}{(p_0/M)^{1/2}}\times[i\gamma_\mu e+i\sigma_{\mu\nu}(p-p')_\nu F_2(W)]\frac{u(p')}{(p_0'/M)^{1/2}}. \quad (1)$$

Similarly the πNN vertex is given by

$$\langle p|j(0)|p'\rangle=\frac{\sqrt{2}\bar{u}(p)}{(p_0/M)^{1/2}}[i\gamma_5\tau G(W)]\frac{u(p')}{(p_0'/M)^{1/2}}. \quad (2)$$

[1] J. M. Cornwall and S. H. Patil, Phys. Rev. Letters **18**, 757 (1967).
[2] See, e.g., M. Gell-Mann, Phys. Rev. **125**, 1067 (1962).
[3] A. Bincer, Phys. Rev. **118**, 885 (1960).